Supervised Learning With Quantum-Inspired Tensor Networks

E. Miles Stoudenmire[1, 2] and David J. Schwab[3]

[1] *Perimeter Institute for Theoretical Physics, Waterloo, Ontario, N2L 2Y5, Canada*
[2] *Department of Physics and Astronomy, University of California, Irvine, CA 92697-4575 USA*
[3] *Dept. of Physics, Northwestern University, Evanston, IL*

(Dated: May 22, 2017)

Tensor networks are efficient representations of high-dimensional tensors which have been very successful for physics and mathematics applications. We demonstrate how algorithms for optimizing such networks can be adapted to supervised learning tasks by using matrix product states (tensor trains) to parameterize models for classifying images. For the MNIST data set we obtain less than 1% test set classification error. We discuss how the tensor network form imparts additional structure to the learned model and suggest a possible generative interpretation.

I. INTRODUCTION

The connection between machine learning and statistical physics has long been appreciated [1–9], but deeper relationships continue to be uncovered. For example, techniques used to pre-train neural networks [8] have more recently been interpreted in terms of the renormalization group [10]. In the other direction there has been a sharp increase in applications of machine learning to chemistry, material science, and condensed matter physics [11–19], which are sources of highly-structured data and could be a good testing ground for machine learning techniques.

A recent trend in both physics and machine learning is an appreciation for the power of tensor methods. In machine learning, tensor decompositions can be used to solve non-convex optimization tasks [20, 21] and make progress on many other important problems [22–24], while in physics, great strides have been made in manipulating large vectors arising in quantum mechanics by decomposing them as *tensor networks* [25–27]. The most successful types of tensor networks avoid the curse of dimensionality by incorporating only low-order tensors, yet accurately reproduce very high-order tensors through a particular geometry of tensor contractions [27].

Another context where very large vectors arise is in non-linear kernel learning, where input vectors $\mathbf{x}$ are mapped into a higher dimensional space via a feature map $\Phi(\mathbf{x})$ before being classified by a decision function

$$f(\mathbf{x}) = W \cdot \Phi(\mathbf{x}) \ . \tag{1}$$

The feature vector $\Phi(\mathbf{x})$ and weight vector W can be exponentially large or even infinite. One approach to deal with such large vectors is the well-known kernel trick, which only requires working with scalar products of feature vectors, allowing these vectors to be defined only implicitly [28].

FIG. 1. The matrix product state (MPS) decomposition, also known as a tensor train. Lines represent tensor indices and connecting two lines implies summation. For an introduction to this graphical tensor notation see Appendix A.

In what follows we propose a rather different approach. For certain learning tasks and a specific class of feature map Φ, we find the optimal weight vector W can be approximated as a tensor network, that is, as a contracted sequence of low-order tensors. Representing W as a tensor network and optimizing it directly (without passing to the dual representation) has many interesting consequences. Training the model scales linearly in the training set size; the cost for evaluating an input is independent of training set size. Tensor networks are also adaptive: dimensions of tensor indices internal to the network grow and shrink during training to concentrate resources on the particular correlations within the data most useful for learning. The tensor network form of W presents opportunities to extract information hidden within the trained model and to accelerate training by using techniques such as optimizing different internal tensors in parallel [29]. Finally, the tensor network form is an additional type of regularization beyond the choice of feature map, and could have interesting consequences for generalization.

One of the best understood types of tensor networks is the matrix product state [26, 30], also known as the tensor train decomposition [31]. Matrix product states (MPS) have been very useful for studying quantum systems, and have recently been proposed for machine learning applications such as learning features of images [23] and compressing the weight layers of neural networks [24]. Though MPS are best suited for describing one-dimensional systems, they are powerful enough to be applied to higher-dimensional systems as well.

There has been intense research into generalizations of MPS better suited for higher dimensions and critical systems [32–34]. Though our proposed approach could generalize to these other types of tensor networks, as a proof of principle we will only consider the MPS decomposition in what follows. The MPS decomposition approximates an order-N tensor by a contracted chain of N lower-order tensors shown in Fig. 1. (Throughout we will use tensor diagram notation; for a brief review see Appendix A.)

Representing the weights W of Eq. (1) as an MPS allows us to efficiently optimize these weights and adaptively change their number by varying W locally a few tensors at a time, in close analogy to the density matrix renormalization group algorithm used in physics [26, 35]. Similar alternating least squares methods for tensor trains have also been explored in applied mathematics [36].

This paper is organized as follows: we propose our general approach then describe an algorithm for optimizing the weight vector W in MPS form. We test our approach, both on the MNIST handwritten digit set and on two-dimensional toy data to better understand the role of the local feature-space dimension d. Finally, we discuss the class of functions realized by our proposed models as well as a possible generative interpretation.

Those wishing to reproduce our results can find sample codes based on the ITensor library [37] at: https://github.com/emstoudenmire/TNML

II. ENCODING INPUT DATA

The most successful use of tensor networks in physics so far has been in quantum mechanics, where combining N independent systems corresponds to taking the tensor product of their individual state vectors. With the goal of applying similar tensor networks to machine learning, we choose a feature map of the form

$$\Phi^{s_1 s_2 \cdots s_N}(\mathbf{x}) = \phi^{s_1}(x_1) \otimes \phi^{s_2}(x_2) \otimes \cdots \phi^{s_N}(x_N) \ . \quad (2)$$

The tensor $\Phi^{s_1 s_2 \cdots s_N}$ is the tensor product of the same local feature map $\phi^{s_j}(x_j)$ applied to each input x_j, where the indices s_j run from 1 to d; the value d is known as the local dimension. Thus each x_j is mapped to a d-dimensional vector, which we require to have unit norm; this implies each $\Phi(\mathbf{x})$ also has unit norm.

The full feature map $\Phi(\mathbf{x})$ can be viewed as a vector in a d^N-dimensional space or as an order-N tensor. The tensor diagram for $\Phi(\mathbf{x})$ is shown in Fig. 2. This type of tensor is said be rank-1 since it is manifestly the product of N order-1 tensors. In physics terms, $\Phi(\mathbf{x})$ has the same structure as a product state or unentangled wavefunction.

For a concrete example of this type of feature map, consider inputs which are grayscale images with N pixels, where each pixel value ranges from 0.0 for white to 1.0 for black. If the grayscale pixel value of the j^{th} pixel is $x_j \in [0, 1]$, a simple choice for the local feature map $\phi^{s_j}(x_j)$ is

$$\phi^{s_j}(x_j) = \left[\cos\left(\frac{\pi}{2}x_j\right),\ \sin\left(\frac{\pi}{2}x_j\right)\right] \quad (3)$$

and is illustrated in Fig. 3. The full image is represented as a tensor product of these local vectors. From a physics perspective, ϕ^{s_j} is the normalized wavefunction of a single qubit where the "up" state corresponds to a white pixel, the "down" state to a black pixel, and a superposition corresponds to a gray pixel.

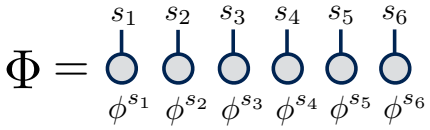

FIG. 2. Input data is mapped to a normalized order N tensor with a trivial (rank 1) product structure.

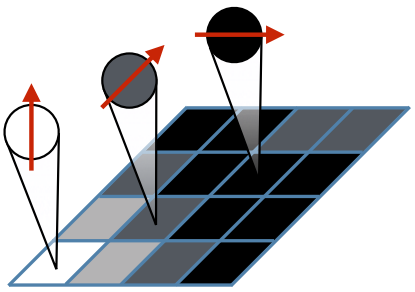

FIG. 3. For the case of a grayscale image and $d = 2$, each pixel value is mapped to a normalized two-component vector. The full image is mapped to the tensor product of all the local pixel vectors as shown in Fig. 2.

While our choice of feature map $\Phi(\mathbf{x})$ was originally motivated from a physics perspective, in machine learning terms, the feature map Eq. (2) defines a kernel which is the product of N local kernels, one for each component x_j of the input data. Kernels of this type have been discussed previously [38, p. 193] and have been argued to be useful for data where no relationship is assumed between different components of the input vector prior to learning [39].

Though we will use only the local feature map Eq. (3) in our MNIST experiment below, it would be interesting to try other local maps and to understand better the role they play in the performance of the model and the cost of optimizing the model.

III. MULTIPLE LABEL CLASSIFICATION

In what follows we are interested in multi-class learning, for which we choose a "one-versus-all" strategy, which we take to mean generalizing the decision function Eq. (4) to a set of functions indexed by a label ℓ

$$f^{\ell}(\mathbf{x}) = W^{\ell} \cdot \Phi(\mathbf{x}) \quad (4)$$

and classifying an input $\mathbf{x}$ by choosing the label ℓ for which $|f^{\ell}(\mathbf{x})|$ is largest.

Since we apply the same feature map Φ to all input data, the only quantity that depends on the label ℓ is the weight vector W^{ℓ}. Though one can view W^{ℓ} as a collection of vectors labeled by ℓ, we will prefer to view W^{ℓ} as an order $N+1$ tensor where ℓ is a tensor index and

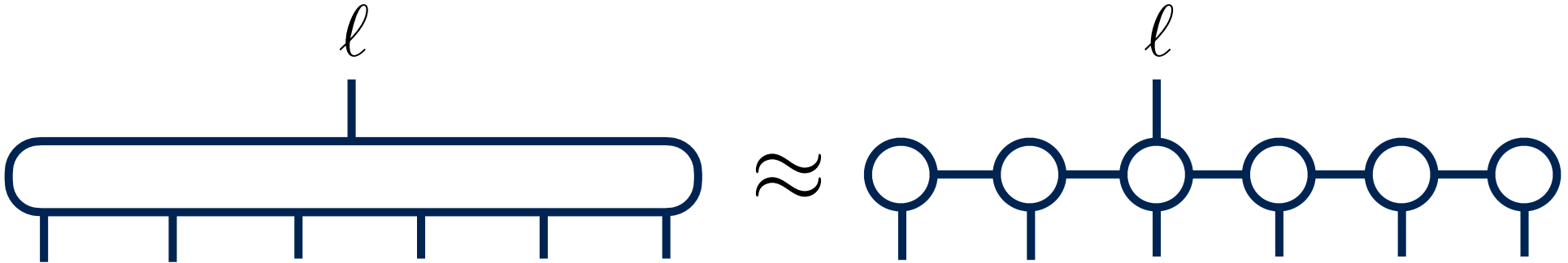
ℓ
$\approx$
ℓ

(a)

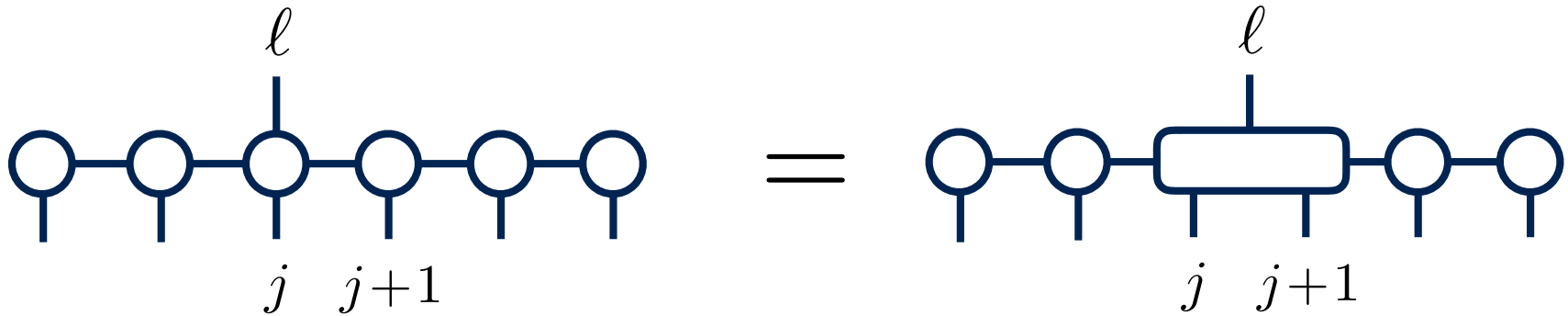

(b)

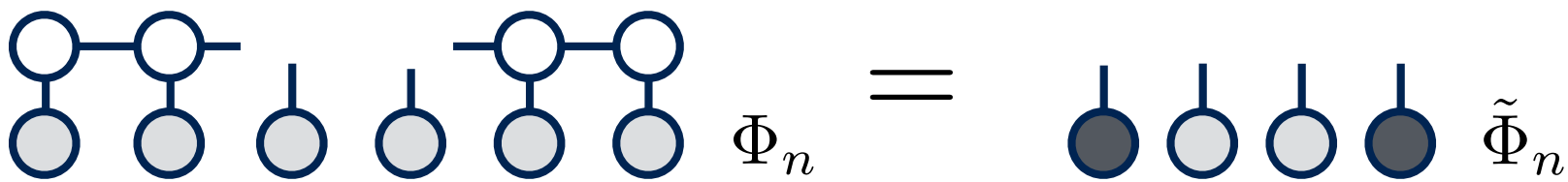

(c)

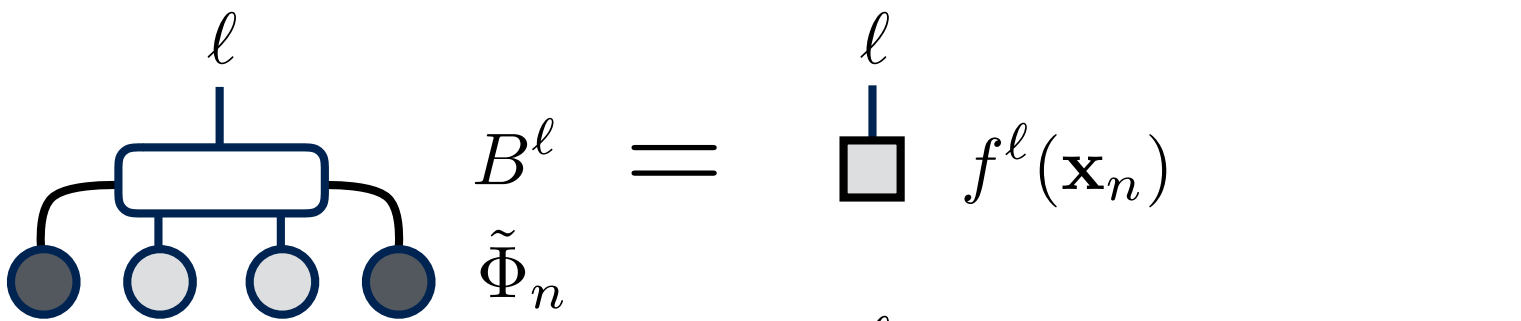

(d)

$$\Delta B^\ell = \sum_n$$

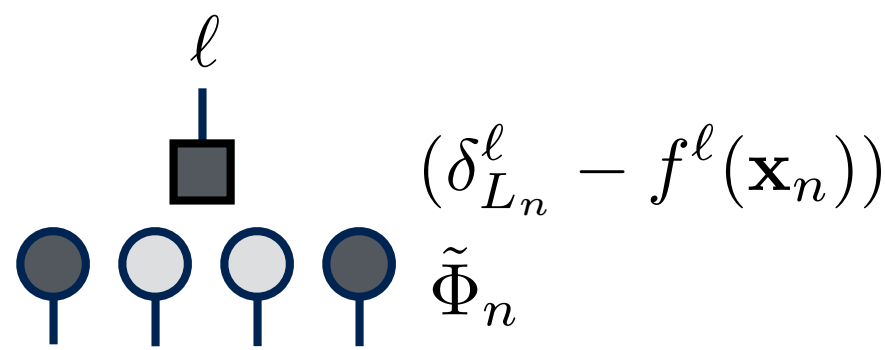

MPS tensor set from a unitary matrix after the SVD as shown in Fig. 7(c). This allows the cost of each local step of the algorithm to remain independent of the size of the input space, making the total algorithm scale only linearly with input space size.

The above algorithm highlights a key advantage of MPS and tensor networks relevant to machine learning applications. Following the SVD of the improved bond tensor B'^{ℓ}, the dimension of the new MPS bond can be chosen *adaptively* based on number of large singular values (defined by a threshold chosen in advance). Thus the MPS form of W^{ℓ} can be compressed as much as possible, and by different amounts on each bond, while still ensuring an optimal decision function.

The scaling of the above algorithm is $d^3\, m^3\, N\, N_L\, N_T$, where recall m is the MPS bond dimension; N the number of input components; N_L the number of labels; and N_T the number of training inputs. In practice, the cost is dominated by the large number of training inputs N_T, so it would be very desirable to reduce this cost. One solution could be to use stochastic gradient descent, but while our experiments at blending this approach with the MPS sweeping algorithm often reached single-digit classification errors, we could not match the accuracy of the full gradient. Mixing stochastic gradient with MPS sweeping thus appears to be non-trivial but we believe it is a promising direction for further research.

Finally, we note that a related optimization algorithm was proposed for hidden Markov models in Ref. 43. However, in place of our SVD above, Ref. 43 uses a non-negative matrix factorization. In a setting where negative weights are allowed, the SVD is the optimal choice because it minimizes the distance between the original tensor and product of factorized tensors. Furthermore, our framework for sharing weights across multiple labels and our use of local feature maps has interesting implications for training performance and for generalization.

VI. MNIST HANDWRITTEN DIGIT TEST

To test the tensor network approach on a realistic task, we used the MNIST data set, which consists of grayscale images of the digits zero through nine [44]. The calculations were implemented using the ITensor library [37]. Each image was originally 28×28 pixels, which we scaled down to 14×14 by averaging clusters of four pixels; otherwise we performed no further modifications to the training or test sets. Working with smaller images reduced the time needed for training, with the tradeoff being that less information was available for learning.

To approximate the classifier tensors as MPS, one must choose a one-dimensional ordering of the local indices $s_1, s_2, \ldots, s_N$. We chose a "zig-zag" ordering shown in Fig. 8, which on average keeps spatially neighboring pixels as close to each other as possible along the one-dimensional MPS path. We then mapped each grayscale image $\mathbf{x}$ to a tensor $\Phi(\mathbf{x})$ using the local map Eq. (3).

FIG. 8. One-dimensional ordering of pixels used to train MPS classifiers for the MNIST data set (after shrinking images to 14×14 pixels).

Using the sweeping algorithm in Section V to train the weights, we found the algorithm quickly converged in the number of passes, or sweeps over the MPS. Typically only two or three sweeps were needed to see good convergence, with test error rates changing only hundreths of a percent thereafter.

Test error rates also decreased rapidly with the maximum MPS bond dimension m. For $m = 10$ we found both a training and test error of about 5%; for $m = 20$ the error dropped to only 2%. The largest bond dimension we tried was $m = 120$, where after three sweeps we obtained a test error of 0.97% (97 misclassified images out of the test set of 10,000 images); the training set error was 0.05% or 32 misclassified images.

VII. TWO-DIMENSIONAL TOY MODEL

To better understand the modeling power and regularization properties of the class of models presented in Sections II and III, consider a family of toy models where the input space is two-dimensional ($N = 2$). The hidden distribution we want to learn consists of two distributions, $P_A(x_1, x_2)$ and $P_B(x_1, x_2)$, from which we generate training data points labeled A or B respectively. For simplicity we only consider the square region $x_1 \in [0, 1]$ and $x_2 \in [0, 1]$.

To train the model, each training point (x_1, x_2) is mapped to a tensor

$$\Phi(x_1, x_2) = \phi^{s_1}(x_1) \otimes \phi^{s_2}(x_2) \tag{12}$$

and the full weight tensors $W^{\ell}_{s_1 s_2}$ for $\ell \in \{A, B\}$ are optimized directly using gradient descent.

When selecting a model, our main control parameter is the dimension d of the local indices s_1 and s_2. For the case $d = 2$, the local feature map is chosen as in Eq. 3. For $d > 2$ we generalize $\phi^{s_j}(x_j)$ to be a normalized d-component vector as described in Appendix B.

A. Regularizing By Local Dimension d

To understand how the flexibility of the model grows with increasing d, consider the case where P_A and P_B are overlapping distributions. Specifically, we take each to be a multivariate Gaussian centered respectively in

the lower-right and upper-left of the unit square, and to have different covariance matrices. In Fig. 9 we show the theoretically optimal decision boundary that best separates A points (crosses, red region) from B points (squares, blue region), defined by the condition $P_A(x_1, x_2) = P_B(x_1, x_2)$. To make a training set, we sample 100 points from each of the two distributions.

Next, we optimize the toy model for our overlapping training set for various d. The decision boundary learned by the $d = 2$ model in Fig. 10(a) shows good agreement with the optimal one in Fig. 9. Because the two sets are non-separable and this model is apparently well regularized, some of the training points are necessarily misclassified—these points are colored white in the figure.

The $d = 3$ decision boundary shown in Fig. 10 begins to show evidence of overfitting. The boundary is more complicated than for $d = 2$ and further from the optimal boundary. Finally, for a much larger local dimension $d = 6$ there is extreme overfitting. The decision boundary is highly irregular and is more reflective of the specific sampled points than the underlying distribution. Some of the overfitting behavior reveals the structure of the model; at the bottom and top of Fig. 10(c) there are lobes of one color protruding into the other. These likely indicate that the finite local dimension still somewhat regularizes the model; otherwise it would be able to overfit even more drastically by just surrounding each point with a small patch of its correct color.

B. Non-Linear Decision Boundary

To test the ability of our proposed class of models to learn highly non-linear decision boundaries, consider the spiral shaped boundary in Fig. 11(a). Here we take P_A and P_B to be non-overlapping with P_A uniform on the red region and P_B uniform on the blue region.

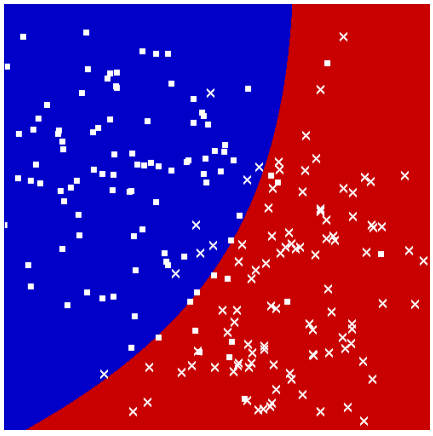

FIG. 9. Training points sampled from multivariate Gaussian distributions $P_A(x_1, x_2)$ [crosses] and $P_B(x_1, x_2)$ [squares]. The curve separating the red A region from the blue B region is the theoretically optimal decision boundary.

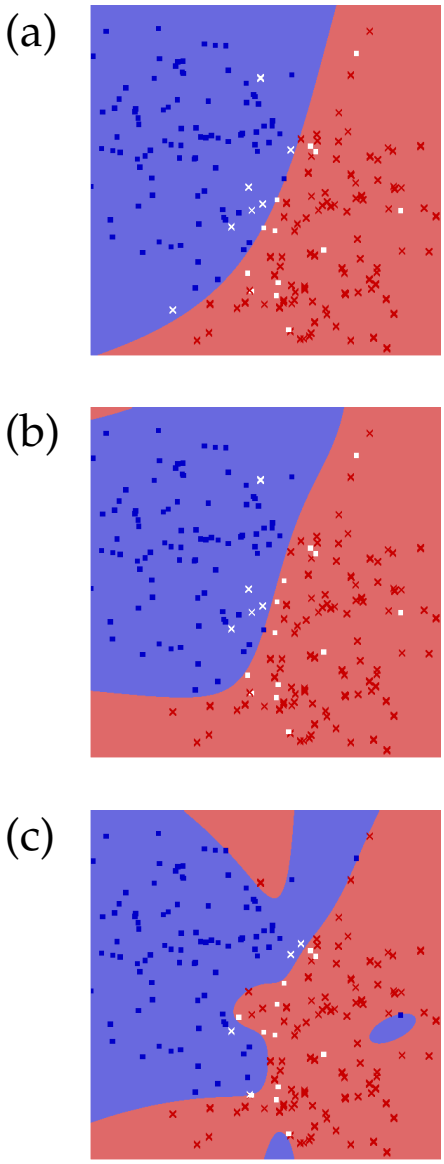

FIG. 10. Toy models learned from the overlapping data set Fig. 9. The results shown are for local dimension (a) $d = 2$, (b) $d = 3$, and (c) $d = 6$. Background colors show how every spatial point would be classified. Misclassified data points are colored white.

In Fig. 11(b) we show the result of training a model with local dimension $d = 10$ on 500 sampled points, 250 for each region (crosses for region A, squares for region B). The learned model is able to classify every training point correctly, though with some overfitting apparent near regions with too many or too few sampled points.

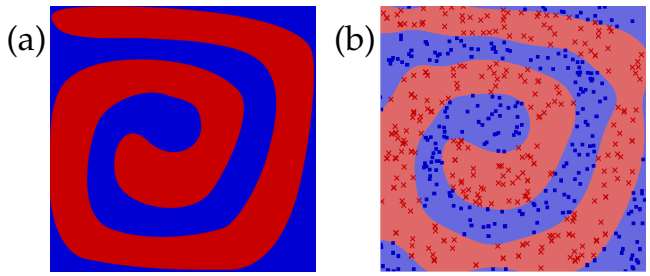

FIG. 11. Toy model reconstruction of interlocking spiral-shaped distribution: (a) original distribution and (b) sampled points and distribution learned by model with local dimension $d = 10$.

VIII. INTERPRETING TENSOR NETWORK MODELS

A natural question is which set of functions of the form $f^\ell(\mathbf{x}) = W^\ell \cdot \Phi(\mathbf{x})$ can be realized when using a tensor-product feature map $\Phi(\mathbf{x})$ of the form Eq. (2) and a tensor-network decomposition of W^ℓ. As we will argue, the possible set of functions is quite general, but taking the tensor network structure into account provides additional insights, such as determining which features the model actually uses to perform classification.

A. Representational Power

To simplify the question of which decision functions can be realized for a tensor-product feature map of the form Eq. (2), let us fix ℓ to a single label and omit it from the notation. We will also consider W to be a completely general order-N tensor with no tensor network constraint. Then $f(\mathbf{x})$ is a function of the form

$$f(\mathbf{x}) = \sum_{\{s\}} W_{s_1 s_2 \cdots s_N} \phi^{s_1}(x_1) \otimes \phi^{s_2}(x_2) \otimes \cdots \phi^{s_N}(x_N) \,. \tag{13}$$

If the functions $\{\phi^s(x)\}$, $s = 1, 2, \ldots, d$ form a basis for a Hilbert space of functions over $x \in [0, 1]$, then the tensor product basis

$$\phi^{s_1}(x_1) \otimes \phi^{s_2}(x_2) \otimes \cdots \phi^{s_N}(x_N) \tag{14}$$

forms a basis for a Hilbert space of functions over $\mathbf{x} \in [0, 1]^{\times N}$. Moreover, if the basis $\{\phi^s(x)\}$ is complete, then the tensor product basis is also complete and $f(\mathbf{x})$ can be any square integrable function.

Next, consider the effect of restricting the local dimension to $d = 2$ as in the local feature map of Eq. (3) which was used to classify grayscale images in our MNIST benchmark in Section VI. Recall that for this choice of $\phi(x)$,

$$\phi(0) = [1,\ 0] \tag{15}$$
$$\phi(1) = [0,\ 1] \,. \tag{16}$$

Thus if $\hat{\mathbf{x}}$ is a black and white image with pixel values of only $\hat{x}_j = \{0, 1\}$, then $f(\hat{\mathbf{x}})$ is equal to a single component $W_{s_1 s_2 \ldots s_N}$ of the weight tensor. Because each of these components is an independent parameter (assuming no further approximation of W), $f(\hat{\mathbf{x}})$ is a highly non-linear, in fact arbitrary, function when restricted to these black and white images.

Returning to the case of grayscale images $\mathbf{x}$ with pixels $x_j \in [0, 1]$, $f(\mathbf{x})$ cannot be an arbitrary function over this larger space of images for finite d. For example, if one considers the $d = 2$ feature map Eq. (3), then when considering the dependence of $f(\mathbf{x})$ on only a single pixel x_j (all other pixels being held fixed), it has the functional form $a\cos(\pi/2\, x_j) + b\sin(\pi/2\, x_j)$ where a and b are constants determined by the (fixed) values of the other pixels.

B. Implicit Feature and Kernel Selection

Of course we have not been considering an arbitrary weight tensor W^ℓ but instead approximating the weight tensor as an MPS tensor network. The MPS form implies that the decision function $f^\ell(\mathbf{x})$ has interesting additional structure. One way to analyze this structure is to separate the MPS into a central tensor, or core tensor $C^{\alpha_i \ell \alpha_{i+1}}$ on some bond i and constrain all MPS site tensors to be *left orthogonal* for sites $j \le i$ or *right orthogonal* for sites $j \ge i$. This means W^ℓ has the decomposition

$$W^\ell_{s_1 s_2 \cdots s_N} = \sum_{\{\alpha\}} U^{\alpha_1}_{s_1} \cdots U^{\alpha_i}_{\alpha_{i-1} s_i} C^\ell_{\alpha_i \alpha_{i+1}} V^{\alpha_{i+1}}_{s_{i+1} \alpha_{i+2}} \cdots V^{\alpha_{N-1}}_{s_N} \tag{17}$$

as illustrated in Fig. 12(a). To say the U and V tensors are left or right orthogonal means when viewed as matrices $U_{\alpha_{j-1} s_j}{}^{\alpha_j}$ and $V^{\alpha_{j-1}}{}_{s_j \alpha_j}$ these tensors have the property $U^\dagger U = I$ and $V V^\dagger = I$ where I is the identity; these orthogonality conditions can be understood more clearly in terms of the diagrams in Fig. 12(b). Any MPS can be brought into the form Eq. (17) through an efficient sequence of tensor contractions and SVD operations similar to the steps in Fig. 7(b).

The form in Eq. (17) suggests an interpretation where the decision function $f^\ell(\mathbf{x})$ acts in three stages. First, an input $\mathbf{x}$ is mapped into the exponentially larger feature space defined by $\Phi(\mathbf{x})$. Next, the d^N dimensional feature vector Φ is mapped into a much smaller m^2 dimensional space by contraction with all the U and V site tensors of the MPS. This second step defines a new feature map $\tilde{\Phi}(\mathbf{x})$ with m^2 components as illustrated in Fig. 12(c). Finally, $f^\ell(\mathbf{x})$ is computed by contracting $\tilde{\Phi}(\mathbf{x})$ with C^ℓ.

To justify calling $\tilde{\Phi}(\mathbf{x})$ a feature map, it follows from the left- and right-orthogonality conditions of the U and V tensors of the MPS Eq. (17) that the indices α_i and α_{i+1} of the core tensor C label an orthonormal basis for

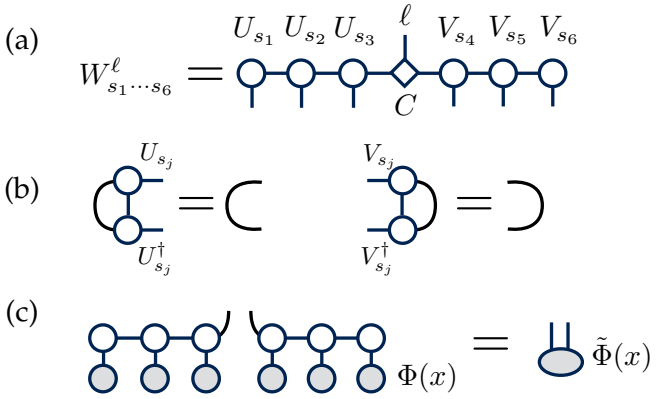

FIG. 12. (a) Decomposition of W^{ℓ} as an MPS with a central tensor and orthogonal site tensors. (b) Orthogonality conditions for U and V type site tensors. (c) Transformation defining a reduced feature map $\tilde{\Phi}(\mathbf{x})$.

a subspace of the original feature space. The vector $\tilde{\Phi}(\mathbf{x})$ is the projection of $\Phi(\mathbf{x})$ into this subspace.

The above interpretation implies that training an MPS model uncovers a relatively small set of important features and simulatenously learns a decision function based only on these reduced features. This picture is similar to popular interpretations of the hidden and output layers of shallow neural network models [45]. A similar interpretation of an MPS as learning features was first proposed in Ref. 23, though with quite a different scheme for representing data than what is used here. It is also interesting to note that an interpretation of the U and V tensors as combining and projecting features into only the m most important combinations can be applied at any bond of the MPS. For example, the tensor $U^{\alpha_{j+1}}_{\alpha_j s_j}$ tensor at site j can be viewed as defining a vector of m features labeled by α_{j+1} by forming linear combinations of products of the features $\phi^{s_j}(x_j)$ and the features α_j defined by the previous U tensor, similar to the contraction in Fig. 7(c).

C. Generative Interpretation

Because MPS were originally introduced to represent wavefunctions of quantum systems [30], it is tempting to interpret a decision function $f^{\ell}(\mathbf{x})$ with an MPS weight vector as a wavefunction. This would mean interpreting $|f^{\ell}(\mathbf{x})|^2$ for each fixed ℓ as a probability distribution function over the set of inputs $\mathbf{x}$ belonging to class ℓ. A major motivation for this interpretation would be that many insights from physics could be applied to machine learned models. For example, tensor networks in the same family as MPS, when viewed as defining a probability distribution, can be used to efficiently perform perfect sampling of the distribution they represent [46].

Let us investigate the properties of W^{ℓ} and $\Phi(\mathbf{x})$ required for a consistent interpretation of $|f^{\ell}(\mathbf{x})|^2$ as a probability distribution. For $|f^{\ell}(\mathbf{x})|^2$ to behave like a probability distribution for a broad class of models, we require for some integration measure $d\mu(x)$ that the distribution is normalized as

$$\sum_{\ell} \int_{\mathbf{x}} |f^{\ell}(\mathbf{x})|^2 d\mu(x) = 1 \tag{18}$$

no matter what weight vector W^{ℓ} the model has, as long as the weights are normalized as

$$\sum_{\ell} \sum_{s_1,s_2,\ldots,s_N} \bar{W}^{\ell}_{s_1 s_2 \cdots s_N} W^{\ell}_{s_1 s_2 \cdots s_N} = 1 \ . \tag{19}$$

This condition is automatically satisfied for tensor-product feature maps $\Phi(\mathbf{x})$ of the form Eq. (2) if the constituent local maps $\phi^s(x)$ have the property

$$\int_x \bar{\phi}^s(x)\phi^{s'}(x)\, d\mu(x) = \delta_{ss'}, \tag{20}$$

that is, if the components of ϕ^s are orthonormal functions with respect to the measure $d\mu(x)$. Furthermore, if one wants to demand, after mapping to feature space, that any input $\mathbf{x}$ itself defines a normalized distribution, then we also require the local vectors to be normalized as

$$\sum_{s} |\phi^s(x)|^2 = 1 \tag{21}$$

for all $x \in [0, 1]$.

Unfortunately neither the local feature map Eq. (3) nor its generalizations in Appendix B meet the first criterion Eq. (20). A different choice that satisfies both the orthogonality condition Eq. (20) and normalization condition Eq. (21) could be

$$\phi(x) = \big[\cos(\pi x),\ \sin(\pi x)\big] \ . \tag{22}$$

However, this map is not suitable for inputs like grayscale pixels since it is anti-periodic over the interval $x \in [0, 1]$ and would lead to a periodic probability distribution. An example of an orthogonal, normalized map which is not periodic on $x \in [0, 1]$ is

$$\phi(x) = \left[e^{i(3\pi/2)x} \cos\left(\frac{\pi}{2}x\right),\ e^{-i(3\pi/2)x} \sin\left(\frac{\pi}{2}x\right)\right] . \tag{23}$$

This local feature map meets the criteria Eqs. (20) and (21) if the integration measure chosen to be $d\mu(x) = 2dx$.

As a basic consistency check of the above generative interpretation, we performed an experiment on our toy model of Section VII, using the local feature map Eq. (23). Recall that our toy data can have two possible labels A and B. To test the generative interpretation, we first generated a single, random "hidden" weight tensor W. From this weight tensor we sampled N_s data points in a two step process:

1. Sample a label $\ell = A$ or $\ell = B$ according to the probabilities $P_A = \int_{\mathbf{x}} |f^A(\mathbf{x})|^2 = \sum_{s_1 s_2} |W^A_{s_1 s_2}|^2$ and $P_B = 1 - P_A$.

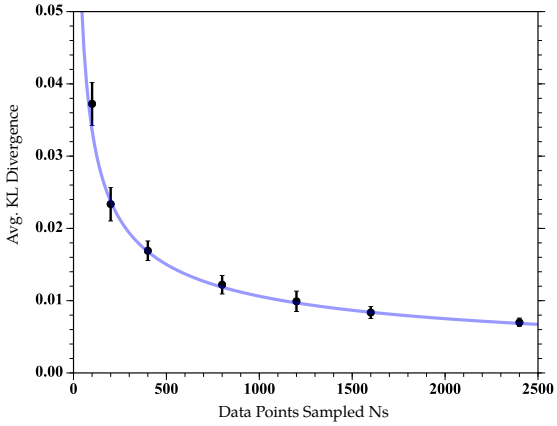

FIG. 13. Average KL divergence between the learned model and original model used to generate data for a two-dimensional toy system as a function of number of sampled training points N_s. The solid curve is a fit of the form $\sigma/\sqrt{N_s}$.

2. Sample a data point $\mathbf{x} = (x_1, x_2)$ according to the distribution $p(\mathbf{x}|\ell) = |f^\ell(\mathbf{x})|^2/P_\ell$ for the chosen ℓ.

For each collection of sampled points we then trained a toy model with weight tensor $\tilde{W}$ using the log-likelihood cost function

$$C = -\sum_{n=1}^{N_s} \log |f^{L_n}(\mathbf{x}_n)|^2 \tag{24}$$

where recall L_n is the known correct label for training point n.

We repeated this procedure multiple times for various sample sizes N_s, each time computing the Kullback-Liebler divergence of the learned versus exact distribution

$$D_{\mathrm{KL}} = \sum_\ell \int_{\mathbf{x}} p(\ell, \mathbf{x}) \log\Big(\frac{p(\ell, \mathbf{x})}{\tilde{p}(\ell, \mathbf{x})}\Big) \tag{25}$$

where $p(\ell, \mathbf{x}) = |f^\ell(\mathbf{x})|^2 = |W^\ell \cdot \Phi(\mathbf{x})|^2$ and $\tilde{p}(\ell, \mathbf{x})$ has similar definition in terms of $\tilde{W}$. The resulting average D_{KL} as a function of number of sampled training points N_s is shown in Fig. 13 along with a fit of the form $\sigma/\sqrt{N_s}$ where σ is a fitting parameter. The results indicate that given enough training data, the learning process can eventually recapture the original probabilistic model that generated the data.

IX. DISCUSSION

We have introduced a framework for applying quantum-inspired tensor networks to multi-class supervised learning tasks. While using an MPS ansatz for the model parameters worked well even for the two-dimensional data in our MNIST experiment, other tensor networks such as PEPS, which are explicitly designed for two-dimensional systems, may be more suitable and offer superior performance. Much work remains to determine the best tensor network for a given domain.

Representing the parameters of our model by a tensor network has many useful and interesting implications. It allows one to work with a family of non-linear kernel learning models with a cost that is linear in the training set size for optimization, and independent of training set size for evaluation, despite using a very expressive feature map (recall in our setup, the dimension of feature space is exponential in the size of the input space). There is much room to improve the optimization algorithm we described, adopting it to incorporate standard tricks such as mini-batches, momentum, or adaptive learning rates. It would be especially interesting to investigate unsupervised techniques for initializing the tensor network.

Additionally, while the tensor network parameterization of a model clearly regularizes it in the sense of reducing the number of parameters, it would be helpful to understand the consquences of this regularization for specific learning tasks. It could also be fruitful to include standard regularizations of the parameters of the tensor network, such as weight decay or L_1 penalties. We were surprised to find good generalization without using explicit parameter regularization. For issues of interpretability, the fact that tensor networks are composed only of linear operations could be extremely useful. For example, it is straightforward to determine directions in feature space which are orthogonal to (or projected to zero by) the weight tensor W.

There exist tensor network coarse-graining approaches for purely classical systems [47, 48], which could possibly be used instead of our approach. However, mapping the data into an extremely high-dimensional Hilbert space is likely advantageous for producing models sensitive to high-order correlations among features. We believe there is great promise in investigating the power of quantum-inspired tensor networks for many other machine learning tasks.

Note: while preparing our final manuscript, Novikov et al. [49] published a related framework for parameterizing supervised learning models with MPS (tensor trains).

Acknowledgments

We would like to acknowledge helpful discussions with Juan Carrasquilla, Josh Combes, Glen Evenbly, Bohdan Kulchytskyy, Li Li, Roger Melko, Pankaj Mehta, U. N. Niranjan, Giacomo Torlai, and Steven R. White. This research was supported in part by the Perimeter Institute for Theoretical Physics. Research at Perimeter Institute is supported by the Government of Canada through Industry Canada and by the Province of Ontario through the Ministry of Economic Development & Innovation. This research was also supported in part by the Simons Foundation Many-Electron Collaboration.

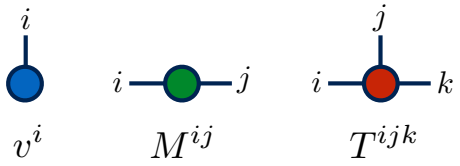

FIG. 14. Graphical tensor notation for (from left to right) a vector, matrix, and order 3 tensor.

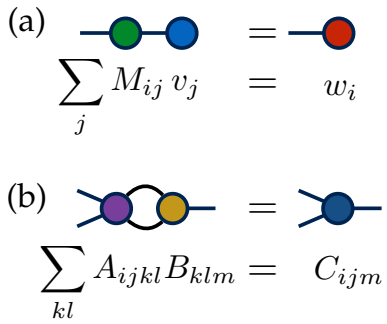

FIG. 15. Tensor diagrams for (a) a matrix-vector multiplication and (b) a more general tensor contraction.

Appendix A: Graphical Notation for Tensor Networks

Though matrix product states (MPS) have a relatively simple structure, more powerful tensor networks, such as PEPS and MERA, have such complex structure that traditional tensor notation becomes unwieldy. For these networks, and even for MPS, it is helpful to use a graphical notation. For some more complete reviews of this notation and its uses in various tensor networks see Ref. 25 and 42.

The basic graphical notation for a tensor is to represent it as a closed shape. Typically this shape is a circle, though other shapes can be used to distinguish types of tensors (there is no standard convention for the choice of shapes). Each index of the tensor is represented by a line emanating from it; an order-N tensor has N such lines. Figure 14 shows examples of diagrams for tensors of order one, two, and three.

To indicate that a certain pair of tensor indices are contracted, they are joined together by a line. For example, Fig. 15(a) shows the contraction of an an order-1 tensor with the an order-2 tensor; this is the usual matrix-vector multiplication. Figure 15(b) shows a more general contraction of an order-4 tensor with an order-3 tensor.

Graphical tensor notation offers many advantages over traditional notation. In graphical form, indices do not usually require names or labels since they can be distinguished by their location in the diagram. Operations such as the outer product, tensor trace, and tensor contraction can be expressed without additional notation; for example, the outer product is just the placement of one tensor next to another. For a network of contracted tensors, the order of the final resulting tensor can be read off by simply counting the number of unpaired lines left over. For example, a complicated set of tensor contractions can be recognized as giving a scalar result if no index lines remain unpaired.

Finally, we note that a related notation for sparse or structured matrices in a direct-sum formalism can be used, and appears extensively in Ref. 50.

Appendix B: Higher-Dimensional Local Feature Map

As discussed in Section II, our strategy for using tensor networks to classify input data begins by mapping each component x_j of the input data vector $\mathbf{x}$ to a d-component vector $\phi^{s_j}(x_j)$, $s_j = 1, 2, \ldots, d$. We always choose $\phi^{s_j}(x_j)$ to be a unit vector in order to apply physics techniques which typically assume normalized wavefunctions.

For the case of $d = 2$ we have used the mapping

$$\phi^{s_j}(x_j) = \left[\cos\left(\frac{\pi}{2}x_j\right), \sin\left(\frac{\pi}{2}x_j\right)\right] . \tag{B1}$$

A straightforward way to generalize this mapping to larger d is as follows. Define $\theta_j = \frac{\pi}{2}x_j$. Because $(\cos^2(\theta_j) + \sin^2(\theta_j)) = 1$, then also

$$(\cos^2(\theta_j) + \sin^2(\theta_j))^{d-1} = 1 . \tag{B2}$$

Expand the above identity using the binomial coeffiecients $\binom{n}{k} = n!/(k!(n-k)!)$.

$$\begin{aligned}(\cos^2(\theta_j) + \sin^2(\theta_j))^{d-1} &= 1 \\ &= \sum_{p=0}^{d-1} \binom{d-1}{p} (\cos\theta_j)^{2(d-1-p)} (\sin\theta_j)^{2p} .\end{aligned} \tag{B3}$$

This motivates defining $\phi^{s_j}(x_j)$ to be

$$\phi^{s_j}(x_j) = \sqrt{\binom{d-1}{s_j-1}}\, (\cos(\frac{\pi}{2}x_j))^{d-s_j} (\sin(\frac{\pi}{2}x_j))^{s_j-1} \tag{B4}$$

where recall that s_j runs from 1 to d. The above definition reduces to the $d = 2$ case Eq. (B1) and guarantees that $\sum_{s_j} |\phi^{s_j}|^2 = 1$ for larger d. (These functions are actually a special case of what are known as *spin coherent states*.)

Using the above mapping $\phi^{s_j}(x_j)$ for larger d allows the product $W^\ell \cdot \Phi(\mathbf{x})$ to realize a richer class of functions. One reason is that a larger local dimension allows the weight tensor to have many more components. Also, for larger d the components of $\phi^{s_j}(x_j)$ contain ever higher frequency terms of the form $\cos\left(\frac{\pi}{2}x_j\right)$, $\cos\left(\frac{3\pi}{2}x_j\right)$, $\ldots$, $\cos\left(\frac{(d-1)\pi}{2}x_j\right)$ and similar terms replacing cos with sin. The net result is that the decision functions realizable for larger d are composed from a more complete basis of functions and can respond to smaller variations in $\mathbf{x}$.

[1] J. J. Hopfield, "Neural networks and physical systems with emergent collective computational abilities," PNAS **79**, 2554–2558 (1982).

[2] Daniel J. Amit, Hanoch Gutfreund, and H. Sompolinsky, "Spin-glass models of neural networks," Phys. Rev. A **32**, 1007–1018 (1985).

[3] Bernard Derrida, Elizabeth Gardner, and Anne Zippelius, "An exactly solvable asymmetric neural network model," EPL (Europhysics Letters) **4**, 167 (1987).

[4] Daniel J. Amit, Hanoch Gutfreund, and H. Sompolinsky, "Information storage in neural networks with low levels of activity," Phys. Rev. A **35**, 2293–2303 (1987).

[5] HS Seung, Haim Sompolinsky, and N Tishby, "Statistical mechanics of learning from examples," Physical Review A **45**, 6056 (1992).

[6] Andreas Engel and Christian Van den Broeck, *Statistical mechanics of learning* (Cambridge University Press, 2001).

[7] Dörthe Malzahn and Manfred Opper, "A statistical physics approach for the analysis of machine learning algorithms on real data," Journal of Statistical Mechanics: Theory and Experiment **2005**, P11001 (2005).

[8] Geoffrey E. Hinton, Simon Osindero, and Yee-Whye Teh, "A fast learning algorithm for deep belief nets," Neural Computation **18**, 1527–1554 (2006).

[9] Marc Mezard and Andrea Montanari, *Information, physics, and computation* (Oxford University Press, 2009).

[10] Pankaj Mehta and David Schwab, "An exact mapping between the variational renormalization group and deep learning," arxiv:1410.3831 (2014).

[11] Christopher C. Fischer, Kevin J. Tibbetts, Dane Morgan, and Gerbrand Ceder, "Predicting crystal structure by merging data mining with quantum mechanics," Nat. Mater. **5**, 641–646 (2006).

[12] Geoffroy Hautier, Christopher C. Fischer, Anubhav Jain, Tim Mueller, and Gerbrand Ceder, "Finding nature's missing ternary oxide compounds using machine learning and density functional theory," Chemistry of Materials **22**, 3762–3767 (2010), http://dx.doi.org/10.1021/cm100795d.

[13] Matthias Rupp, Alexandre Tkatchenko, Klaus-Robert Müller, and O. Anatole von Lilienfeld, "Fast and accurate modeling of molecular atomization energies with machine learning," Phys. Rev. Lett. **108**, 058301 (2012).

[14] Yousef Saad, Da Gao, Thanh Ngo, Scotty Bobbitt, James R. Chelikowsky, and Wanda Andreoni, "Data mining for materials: Computational experiments with *AB* compounds," Phys. Rev. B **85**, 104104 (2012).

[15] John C. Snyder, Matthias Rupp, Katja Hansen, Klaus-Robert Müller, and Kieron Burke, "Finding density functionals with machine learning," Phys. Rev. Lett. **108**, 253002 (2012).

[16] Ghanshyam Pilania, Chenchen Wang, Xun Jiang, Sanguthevar Rajasekaran, and Ramamurthy Ramprasad, "Accelerating materials property predictions using machine learning," Scientific Reports **3**, 2810 EP – (2013).

[17] Louis-François Arsenault, Alejandro Lopez-Bezanilla, O. Anatole von Lilienfeld, and Andrew J. Millis, "Machine learning for many-body physics: The case of the Anderson impurity model," Phys. Rev. B **90**, 155136 (2014).

[18] Mohammad H. Amin, Evgeny Andriyash, Jason Rolfe, Bohdan Kulchytskyy, and Roger Melko, "Quantum Boltzmann machine," arxiv:1601.02036 (2016).

[19] Juan Carrasquilla and Roger G. Melko, "Machine learning phases of matter," Nat Phys **13**, 431–434 (2017).

[20] Animashree Anandkumar, Rong Ge, Daniel Hsu, Sham M. Kakade, and Matus Telgarsky, "Tensor decompositions for learning latent variable models," Journal of Machine Learning Research **15**, 2773–2832 (2014).

[21] Animashree Anandkumar, Rong Ge, Daniel Hsu, and Sham M. Kakade, "A tensor approach to learning mixed membership community models," J. Mach. Learn. Res. **15**, 2239–2312 (2014).

[22] Anh Huy Phan and Andrzej Cichocki, "Tensor decompositions for feature extraction and classification of high dimensional datasets," Nonlinear theory and its applications, IEICE **1**, 37–68 (2010).

[23] J.A. Bengua, H.N. Phien, and H.D. Tuan, "Optimal feature extraction and classification of tensors via matrix product state decomposition," in *2015 IEEE Intl. Congress on Big Data (BigData Congress)* (2015) pp. 669–672.

[24] Alexander Novikov, Dmitry Podoprikhin, Anton Osokin, and Dmitry Vetrov, "Tensorizing neural networks," arxiv:1509.06569 (2015).

[25] Jacob C. Bridgeman and Christopher T. Chubb, "Hand-waving and interpretive dance: An introductory course on tensor networks," arxiv:1603.03039 (2016).

[26] U. Schollwöck, "The density-matrix renormalization group in the age of matrix product states," Annals of Physics **326**, 96–192 (2011).

[27] G. Evenbly and G. Vidal, "Tensor network states and geometry," Journal of Statistical Physics **145**, 891–918 (2011).

[28] K. R. Muller, S. Mika, G. Ratsch, K. Tsuda, and B. Scholkopf, "An introduction to kernel-based learning algorithms," IEEE Transactions on Neural Networks **12**, 181–201 (2001).

[29] E. M. Stoudenmire and Steven R. White, "Real-space parallel density matrix renormalization group," Phys. Rev. B **87**, 155137 (2013).

[30] Stellan Östlund and Stefan Rommer, "Thermodynamic limit of density matrix renormalization," Phys. Rev. Lett. **75**, 3537–3540 (1995).

[31] I. Oseledets, "Tensor-train decomposition," SIAM Journal on Scientific Computing **33**, 2295–2317 (2011).

[32] F. Verstraete and J. I. Cirac, "Renormalization algorithms for quantum-many body systems in two and higher dimensions," cond-mat/0407066 (2004).

[33] G. Vidal, "Entanglement renormalization," Phys. Rev. Lett. **99**, 220405 (2007).

[34] G. Evenbly and G. Vidal, "Algorithms for entanglement renormalization," Phys. Rev. B **79**, 144108 (2009).

[35] Steven R. White, "Density matrix formulation for quantum renormalization groups," Phys. Rev. Lett. **69**, 2863–2866 (1992).

[36] Sebastian Holtz, Thorsten Rohwedder, and Reinhold Schneider, "The alternating linear scheme for tensor optimization in the tensor train format," SIAM Journal on

Scientific Computing **34**, A683–A713 (2012).
[37] ITensor Library (version 2.0.7) http://itensor.org.
[38] Vladimir Vapnik, *The Nature of Statistical Learning Theory* (Springer-Verlag New York, 2000).
[39] W. Waegeman, T. Pahikkala, A. Airola, T. Salakoski, M. Stock, and B. De Baets, "A kernel-based framework for learning graded relations from data," Fuzzy Systems, IEEE Transactions on **20**, 1090–1101 (2012).
[40] E.M. Stoudenmire and Steven R. White, "Studying two-dimensional systems with the density matrix renormalization group," Annual Review of Condensed Matter Physics **3**, 111–128 (2012).
[41] F. Verstraete, D. Porras, and J. I. Cirac, "Density matrix renormalization group and periodic boundary conditions: A quantum information perspective," Phys. Rev. Lett. **93**, 227205 (2004).
[42] Andrzej Cichocki, "Tensor networks for big data analytics and large-scale optimization problems," arxiv:1407.3124 (2014).
[43] Jason T. Rolfe and Matthew Cook, "Multifactor expectation maximization for factor graphs," (Springer Berlin Heidelberg, Berlin, Heidelberg, 2010) pp. 267–276.
[44] Christopher J.C. Burges Yann LeCun, Corinna Cortes, "MNIST handwritten digit database," http://yann.lecun.com/exdb/mnist/ .
[45] Michael Nielsen, *Neural Networks and Deep Learning* (Determination Press, 2015).
[46] Andrew J. Ferris and Guifre Vidal, "Perfect sampling with unitary tensor networks," Phys. Rev. B **85**, 165146 (2012).
[47] Efi Efrati, Zhe Wang, Amy Kolan, and Leo P Kadanoff, "Real-space renormalization in statistical mechanics," Reviews of Modern Physics **86**, 647 (2014).
[48] G. Evenbly and G. Vidal, "Tensor network renormalization," Phys. Rev. Lett. **115**, 180405 (2015).
[49] Alexander Novikov, Mikhail Trofimov, and Ivan Oseledets, "Exponential machines," arxiv:1605.03795 (2016).
[50] Matthew T. Fishman and Steven R. White, "Compression of correlation matrices and an efficient method for forming matrix product states of fermionic gaussian states," Phys. Rev. B **92**, 075132 (2015).